



Influence of Co to Ni ratio in γ' -strengthened model alloys on oxidation resistance and the efficacy of the halogen effect at 900 °C

Martin Weiser^a, Mathias C. Galetz^b, Hans-Eberhard Zschau^b, Christopher H. Zenk^c, Steffen Neumeier^c, Mathias Göken^c, Sannakaisa Virtanen^{a,*}

^a Materials Science and Engineering, Institute for Surface Science and Corrosion, Friedrich-Alexander-Universität Erlangen-Nürnberg (FAU), Martensstr. 7, Erlangen, Germany

^b DECHHEMA-Forschungsinstitut, Theodor-Heuss-Allee 25, Frankfurt am Main, Germany

^c Materials Science and Engineering, Institute I, Friedrich-Alexander-Universität Erlangen-Nürnberg (FAU), Martensstr. 5, Erlangen, Germany

ARTICLE INFO

Keywords:

Oxidation

Co/Ni-base model alloys

Halogen effect

Diffusion-limiting scales

EPMA

ABSTRACT

The role of base element (Co or Ni) in γ' -strengthened single-crystalline superalloys was elucidated in the present study. Reaction kinetics during oxidation at 900 °C were assessed by thermogravimetry and measurements of individual layer thicknesses in the multilayered oxide scales. The development of diffusion-limiting barrier layers as well as the extent of sub-scale phase transitions could be directly correlated to the Co/Ni ratio in the alloy. For the first time a surface pretreatment with F was applied to Co-base superalloys. Apparent differences in the efficacy of the halogen effect depending on the Co content in the model alloys were observed.

1. Introduction

Ni-base superalloys are commonly used as material for load-bearing components such as turbine blades at high temperatures. With service conditions approaching the solidus temperature of Ni-base superalloys, the maximum operation temperature in state-of-the-art gas turbines is reaching its limit [1]. Since the discovery of a stable L1₂ phase in the Co-Al-W system by Sato et al. in 2006, Co as potential base material for alloys used in harsh thermal and chemical environments, suddenly gained attention [2]. Several studies on ternary and quaternary γ' -strengthened Co-base superalloys demonstrated higher solidus and liquidus temperatures along with promising mechanical properties such as good creep resistance and high flow stresses at temperatures beyond 900 °C [3–5]. A major issue in the ternary Co-Al-W system remains the long-term stability of the γ/γ' microstructure [4,6]. By the addition of Ni as further alloying element, the decomposition of γ' is suppressed with simultaneous widening of the narrow two-phase field [7].

Even though the resistance against oxidation of quaternary polycrystalline Co-base superalloys at 900 °C could be improved by the addition of 9 and 18 at.% Ni [8], the oxidation properties of these alloys remained substantially poor. In 2016, a mechanistic study revealed strongly varying material properties in a set of polycrystalline Co/Ni-base model alloys with minor B contents when Co was successively

replaced by Ni [9,10]. In order to increase the oxidation resistance, the alloys contained a constant amount of 8 at.% Cr in addition to 9 at.% Al. Irrespective of the Cr content, the oxidation resistance remained unsatisfying. This finding is underlined by the fact, that despite a substantially lower mass gain for compositions with a Co/Ni ratio of 1 and below, none of the investigated specimens showed external Cr₂O₃ and/or Al₂O₃ layers after 100 h exposure at 900 °C in air [9]. A recent study demonstrated the decay of the desired two-phase microstructure in Co-Al-W alloys as consequence of high Cr levels [5]. Furthermore, the narrow stability region of the γ/γ' region in ternary pure Co-base alloys was subject to several investigations [2,7,11]. The tolerable levels of Al and Cr are relatively low on the Co-rich side which also results in unsatisfying oxidation properties above 900 °C in model systems that are composed of up to 5 elements.

A promising strategy to facilitate the external growth of a dense and sustainable Al₂O₃ layer is the surface treatment of Al-containing alloys with halides, such as F and Cl, prior to exposure. In literature, the so-called halogen effect was extensively investigated for TiAl [12–14] and more recently also successfully applied to improve the protective properties Ni-base superalloys with medium Al contents (< 8 at.%) at 1000 °C and above [15–17].

In the present study, the set of single-crystalline intermediate Co/Ni-base model alloys, that was described by Zenk et al. [9] is chosen to

* Corresponding author.

E-mail addresses: martin.weiser@fau.de (M. Weiser), mathias.galetz@dechema.de (M.C., Galetz), zschau@dechema.de (H.-E. Zschau), zenk.7@osu.edu (C.H. Zenk), steffen.neumeier@fau.de (S. Neumeier), mathias.goeken@ww.uni-erlangen.de (M. Göken), virtanen@ww.uni-erlangen.de (S. Virtanen).

perform a mechanistic study of oxide scale growth during exposure at 900 °C in synthetic air. The intention of the work is to understand the reported changes of elementary processes that arise from the increasing Ni content in the alloy system. A deeper understanding of the aforementioned processes is essential for the design of oxidation-resistant high-temperature alloys. The halogen effect as another interesting approach to increase Al activity and efficiently slow down oxide scale growth on alloys with limited amounts of Al and Cr was tested for the entire range of considered compositions.

2. Experimental procedures

2.1. Materials

A set of five different single-crystalline Co/Ni-base model alloys was casted using the Bridgman process by the Institute of Metals Science and Technology (WTM, University of Erlangen-Nürnberg (FAU), Germany). In order to determine actual compositions after heat treatment, pieces of each alloy were dissolved and subsequently characterised by ICP-OES. Acronyms for the investigated alloy systems indicating the Co to Ni ratio were chosen to provide comparability with previous works of the authors [9]. The measured composition along with the individual designations that are used in the course of this work are given in Table 1.

The heat-treatment was conducted in a vacuum tube furnace and included a homogenization step at 1250 °C for 12 h. Subsequent aging was performed for 100 h at 900 °C in the same device. Disc-shaped samples with approximately 0.8 mm height were directly cut from the rod.

2.2. Thermogravimetric analysis

Thermogravimetry was performed using a Setaram Evolution 1650 analyser under constant gas flow of 20 cm³/min. All relevant surfaces of the investigated specimens were ground and polished down to 1 μm surface finish. The atmosphere inside the reaction tube was changed to Ar prior to heating. At the target temperature, the interior of the device was evacuated and refilled with dry synthetic air (80%N₂ + 20%O₂). The detection of mass gain during isothermal oxidation experiments started with the inlet of the oxidising gas.

2.3. Halogen treatment and thermal exposure

The F treatment was performed by using beamline ion-implantation (BLI2). The process is characterised by high precision and reproducibility. A CF₄ gas in a cold cathode plasma source was used for the acceleration of positive F ions. The adjusted ion energy of 38 keV corresponds to a projected range of 35–40 nm in the alloys. All alloys were implanted with a fluence of 1.0×10^{17} F/cm², except NC75sx that was treated with a fluence of 6.4×10^{16} F/cm². These implantation parameters were chosen because of the good results obtained for Ni-base alloys. Only one side was implanted, whereas the untreated side served as comparison. All implantations were performed using the 60 kV ion implanter of the Goethe University Frankfurt. Isothermal exposure of F-

Table 1
Chemical composition (at.%) of the investigated Co/Ni-base model alloys.

Designation	Nominal composition	Measured composition				
		Co	Ni	Al	W	Cr
NC100sx	Co–9Al–8W–8Cr	76.7	0	8.6	7.6	7.1
NC75sx	Co–18.75Ni–9Al–8W–8Cr	57.5	19.8	8.5	7.2	7.1
NC50sx	Co–37.5Ni–9Al–8W–8Cr	37.9	38.9	8.5	8.0	6.9
NC25sx	Co–56.25Ni–9Al–8W–8Cr	18.8	58.1	8.4	7.6	7.3
NC00sx	Ni–9Al–8W–8Cr	0	77.0	8.3	7.7	7.3

treated samples at 900 °C for 100 h was performed at the DECHEMA-Forschungsinstitut.

2.4. Analysis of cross-sections

For subsequent investigation of cross-sections, oxidised samples were protected by an electrochemically deposited Ni layer to minimise spallation. Due to stresses during metallographic preparation of cross sections, Ni layers can detach and are therefore not necessarily visible in the BSE micrograph.

Cross-sections were either prepared using an ion milling system (Hitachi IM4000) or by mechanical grinding and polishing. Due to the considerably higher quality, information on the development of distinct morphological features of the oxide scales were conducted on ion-milled cross-sections in a field-emission scanning electron microscope (FE-SEM, Hitachi S-4800). Backscattered SEM micrographs and the imaging software ImageJ were used to directly determine thicknesses of individual regions. The distribution of elements in oxide scales and subsurface region, after 100 h exposure, was qualitatively assessed by electron probe microanalysis (EPMA, Jeol JXA-8100). Concentration profiles were determined using the same method.

3. Results

3.1. Mass gain and multilayered scale growth at 900 °C

Area-corrected mass gain data of all specimens during isothermal exposure at 900 °C is displayed in Fig. 1.

The thermogravimetric data acquired for the pure Co-base alloy NC100sx, demonstrated only a low degree of reproducibility. The deviation of the data between individual measurements was particularly pronounced during the first 50 h of isothermal exposure. In the graph, a mean value of three experiments is displayed, with error bars indicating the standard deviation of the mass gain values after selected duration of oxidation in addition to the average curve. For all other compositions, the reproducibility of weight gain measurements was sufficiently high. Therefore, only representative data originating from one experiment are displayed for model alloys containing Ni. The reason for the scatter in mass gain is explained in more detail at a later stage of this study. Replacing Co by Ni leads to a significant decrease in mass gain. Differences in the overall behaviour are already visible after 2 h of oxidation. All investigated specimens revealed a period of initially rapid increase in sample weight during the first 20 h of oxide scale growth. Depending on the alloy composition, the prevailing kinetics of oxidation demonstrate remarkable differences. The pure Co-base alloy NC100sx reveals by far the highest mass gain after the entire duration

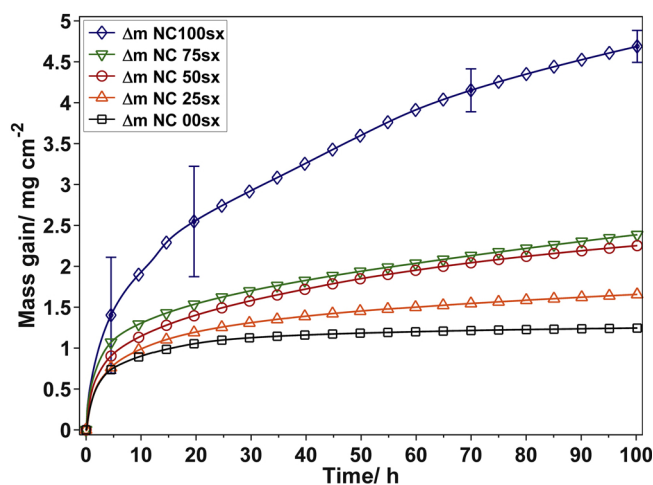


Fig. 1. Mass gain during 100 h oxidation at 900 °C in synthetic air.

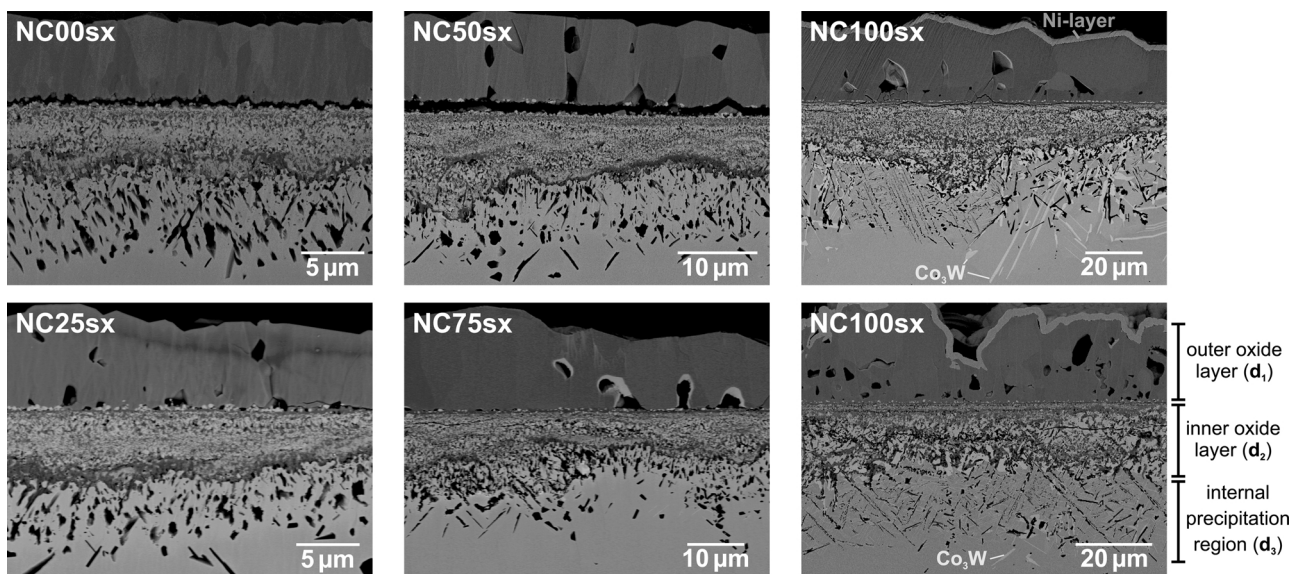


Fig. 2. BSE micrographs of multilayered scales on Co/Ni-base model alloys after 100 h exposure at 900 °C in synthetic air.

of exposure. The average mass gain curve for NC100sx exhibits several sudden declines followed by subsequent moderate increases. In the end, the overall weight change per sample area corresponds to a factor of nearly two higher than for NC75sx and NC50sx. In the case of NC75sx and NC50sx, the kinetics of oxidation are very similar. A mass gain of 1.25 mg/cm² was measured for the pure Ni-base sample NC00sx after 100 h of isothermal exposure. The sample weight of NC00sx reached 90% of its total increase already after 30 h oxidation, while Co-containing samples showed continuous increase with exposure time. During the whole duration of the isothermal experiment, the mass gain of NC25sx demonstrates values between the pure Ni-base alloy NC00sx and NC50sx.

Backscattered electron (BSE) micrographs of all compositions after 100 h thermogravimetric analysis are shown in Fig. 2. In the case of NC100sx, the oxidation behaviour did not only differ between individual specimen, but also demonstrated remarkable changes across the same sample. The two displayed micrographs for NC100sx were taken from different locations of the cross-section observed on the same specimen.

The oxide scales found on Co/Ni-base model alloys exhibited multilayered morphologies, comparable to those developed on polycrystalline samples [9]. Considering the overall thickness of the grown oxide scales, the trend is consistent with the data obtained from thermogravimetric analysis. In other words, the oxide scale observed on NC100sx exhibited the greatest thickness, and the scale on NC00sx, the smallest thickness. Despite the high number of possible different oxide species developed on each individual sample, every scale can be divided into three individual layers. The outer oxide layer (d_1) formed on top of the original alloy surface. Underneath, a mixture of various oxide phases can be summarised as inner oxide layer (d_2). Between the unoxidised alloy and d_2 , a region (d_3) can be seen where isolated phases that appear dark in the BSE micrograph precipitated in the unaffected matrix phase. The average thicknesses (\bar{d}_x) along with the standard deviations ($sd(d_x)$) for the distinguished three layers after 100 h exposure in air at 900 °C are summarised in Table 2.

Not only the size but also the appearance of oxide scales alters considerably when Co is successively replaced by Ni. The overall thicknesses increase towards the Co-rich side. Furthermore, a higher fractional area of the interface between d_2 and d_3 is covered by a layer, that appears dark in the backscatter electron micrographs. The dark layers in the majority of cases found on the d_2/d_3 interfaces are most probably segments of a barrier layer, which appear to only cover part of

Table 2

Mean thicknesses of individually distinguished layers d_1 , d_2 and d_3 after 100 h thermogravimetry at 900 °C in synthetic air. Standard deviations $sd(d_x)$ were determined from 5 independent measurements.

Sample	$\bar{d}_1/\mu m$	$sd(d_1)/\mu m$	$\bar{d}_2/\mu m$	$sd(d_2)/\mu m$	$\bar{d}_3/\mu m$	$sd(d_3)/\mu m$
NC100sx	23.5	8.4	23.0	2.9	21.2	2.7
NC75sx	12.9	1.9	9.3	3.8	10.7	3.4
NC50sx	10.4	1.5	10.0	2.2	8.2	2.5
NC25sx	7.0	0.8	4.9	1.0	6.7	1.7
NC00sx	6.4	0.4	5.2	1.7	6.8	1.3

the exposed surface area of alloys NC100sx and NC75sx after 100 h oxidation. For Ni contents exceeding the amount of Co, the entire subsurface zone is covered by these layers that appear to be almost continuous. The shape of internal precipitates in d_3 found after 100 h oxidation evidently depends on the Co/Ni ratio. In the pure Co-base samples these phases are thin and needle-like, whereas their appearance is mostly globular in the alloy characterised by equal Co and Ni contents. Following the subsequent addition of Ni, a pear-shaped internal precipitates are observed. The originally polished sample surface forms the border between outer oxide layer and internal oxidation zone. As can be seen in Fig. 2, the outer oxide can be prone to detachment. Even though only the outer oxide layer of NC00sx and NC50sx spalled in the displayed micrographs, no clear dependency of scale detachment on the Co/Ni ratio of the specimen could be determined. A relatively homogeneous outer oxide layer can be observed on the pure Ni alloy. Compared to the other scales, smaller grains in d_1 are recognizable in the electron micrograph.

3.2. Elemental distribution

In the presented mass gain data and corresponding cross-sections, the most evident differences could be seen between NC100sx, NC50sx and NC00sx. For a more complete picture, data from NC75sx and NC25sx with a Co to Ni ratio of 3:1 and 1:3, respectively are also taken into consideration where necessary. The primary focus of this study however, is set on the fundamental differences between the pure Co- and Ni-base alloys and the intermediate composition with equal Co and Ni contents.

During the exposure of the pure Co-base alloy NC100sx, the overall reaction kinetics undergo persistent transitions and rather abrupt

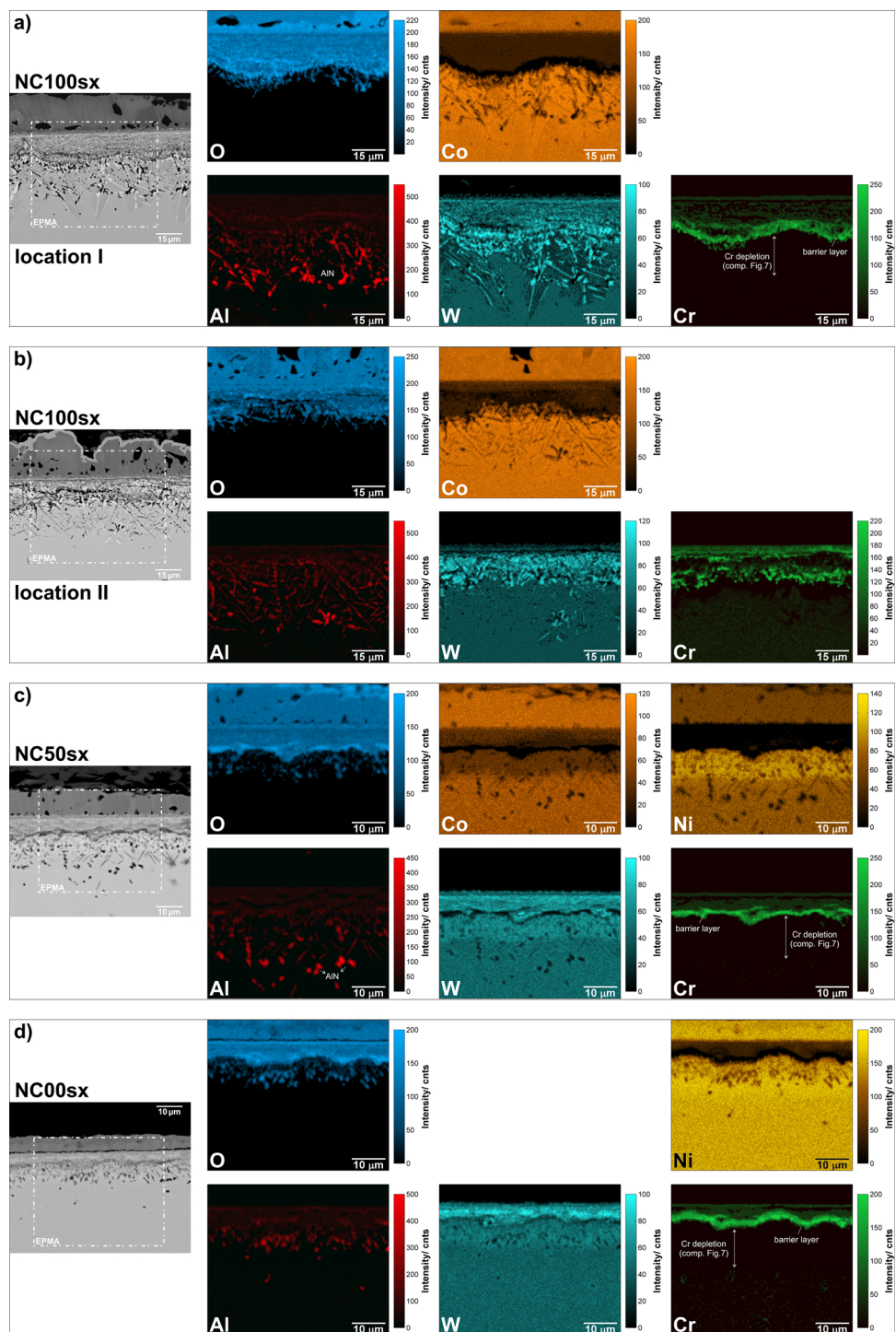


Fig. 3. SE micrographs of oxide scales grown on (a/b) NC100sx, (c) NC50sx and (d) NC00sx during 100 h exposure at 900 °C. Elemental distribution in the marked (—) regions was determined by EPMA.

changes in oxidation rates. Due to the initially high increase in mass, during the first 20 h of exposure, changes are less pronounced in the plot after 50 h, but still evident. All alloys containing Ni do not exhibit these characteristic features over the course of the experiment. The scale growth of polycrystalline Co/Ni-base was reported to follow a nearly parabolic rate after long durations of exposure [9]. The kinetics of oxidation reactions are always related to mass transport, which inevitably causes changes in local composition of the oxide scale and adjacent regions of the alloys. Therefore, information on elemental distribution are needed, to gain essential insights into elementary

mechanisms, that are relevant during the oxide scale growth on Co/Ni-base model alloys.

Fig. 3 shows elemental mappings (EPMA) of regions in the samples NC100sx, NC50sx and NC00sx that are affected by the formation of oxide scales during 100 h exposure. The intention of the displayed mappings is to highlight differences in elemental contents of individual layers in high spatial resolution. Since d_1 , especially for pure Co- or Ni-base alloys is not expected to exhibit measurable deviations from the stoichiometry of the pure Co and Ni oxides which are stable at the investigated temperature, the outer oxide layer is not necessarily included

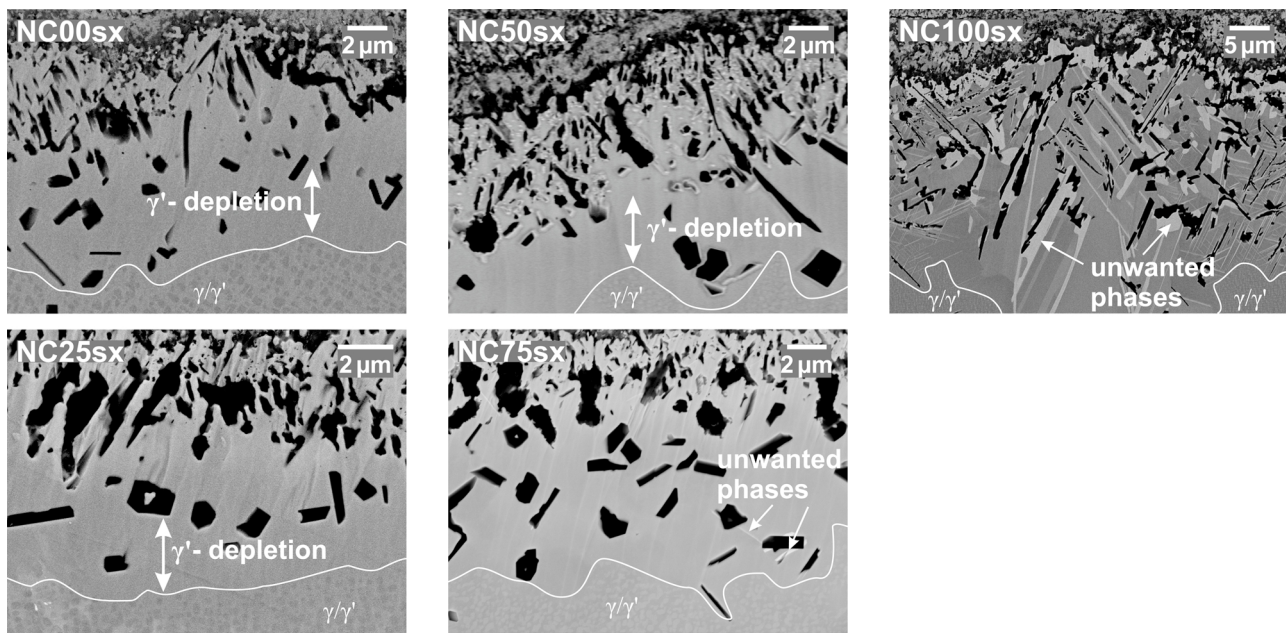


Fig. 4. Appearance of internal oxidation front (IOF) after 100 h exposure at 900 °C.

to its full extent for all specimens.

For NC100sx, two regions of the scale are shown in Fig. 3a and 3 b. The outer oxide layer contains solely O and Co in both cases. Due to the high oxidation temperature, the majority of d_1 is expected to consist of pure CoO. In the inner oxide layer, all alloying elements are found. This layer is a conglomerate of several oxide phases which was already evident in the BSE micrographs (Fig. 2). At the interface between d_2 and d_3 at location I (Fig. 3a), a substantial enrichment of Cr indicates the formation of a Cr-containing barrier layer. At location II enrichment of Cr in d_2 is evident along the interface to d_3 , but also in regions closer to the original alloy surface. Furthermore, the Cr-containing layer along the interface between d_2 and d_3 is not continuous, which facilitates local attack of the alloy by internal oxidation. The distribution of W in d_2 does not exhibit a clear tendency. EPMA line scans (not shown) exhibit also considerable Co levels at the d_2/d_3 interface. The higher intensities in the W maps, visible at both locations, are most likely caused by ongoing depletion of Co that diffuses towards the outer interface to expand d_1 . In d_3 , a significant increase of Al signal is evident. The dark, needle-like phases contain large portions of Al and are accompanied by high W contents in adjacent regions. Al-rich precipitates only exhibit considerable O signal in the top 2–5 μm of d_3 . Below this zone, formation of (Al) nitrides explains the appearance of precipitates with high Al content. The W increase in d_3 indicates the undesired formation of Co_3W phases caused by Al depletion. This phase transition is typical for ternary and quaternary Co-base superalloys with low γ stability. Oxide scales grown on NC75sx (not shown) exhibit comparable layering. Particularly notable is that on the investigated cross-section no indication of a continuous barrier layer could be found.

The oxide scale on NC50sx after 100 h, displayed in Fig. 3c, is more complex due to the addition of Ni as second base element. Considerable amounts of both, Co and Ni can be detected in the outer oxide layer. Even though the Co intensity is higher, it is not possible to make conclusions on the nature of the prevailing oxide in this layer. In d_2 , all elements are included. However, the intensity values for Ni remain relatively low. The distribution of W in NC50sx is mostly unaffected by oxidation during exposure in air. A minor increase in measured intensities is evident in d_2 and the adjacent section of d_3 . This increase is a consequence of Co and Ni diffusion towards the outer interface. A continuous Cr-rich barrier layer is evident on the interface between d_2 and d_3 . In d_3 , Al-rich phases can be determined. Similar to the pure Co-

base alloy, the internal precipitate region is partly composed of AlN.

Oxide scales that are observed on alloys with higher Ni content (NC25sx and NC00sx) are comparable in terms of oxide layer morphology. In Fig. 3d, intensity mappings of all relevant elements in the scale and adjacent regions of NC00sx after 100 h oxidation are displayed. The outer oxide layer developed at 900 °C is assumed to be NiO. Considerable amounts of all elements are found in d_2 . The formation of a continuous Cr-rich barrier layer started only a few microns below the original alloy surface and represents the transition from the inner oxide layer to the internal precipitation region. Considerable depletion of Ni is only noticeable in d_2 . For the pure Ni-base alloys, nearly all Al precipitates in d_3 also exhibit high O intensities and can therefore be identified as internally-oxidised Al_2O_3 or Ni-containing spinels. Lateral spreading of alumina sections can only be observed on very few locations.

3.3. Kinetics of oxide scale growth

BSE micrographs of representative regions surrounding the internal oxidation front (IOF) are shown in Fig. 4 in order to examine the phase stability during thermal exposure in air at 900 °C.

All micrographs were taken after 100 h oxidation and include the interface between d_2 and d_3 in the uppermost region along with unaltered γ/γ' microstructure. Unwanted Co_3W phases as well as considerable depletion of γ are highlighted in the figure. For equal Co and Ni content, W does not partition to a significant extent in either of the two phases. Therefore, additional ion flat milling was used to visualize the γ phase in the cross sections of oxidized NC50sx samples by preferential sputtering of the matrix. In both Co-rich alloys, Co_3W was found contiguous to Al-rich precipitates in d_3 . The W-rich intermetallic phases grew to a large extent in the pure Co-base alloys, whereas only very thin isolated needles occurred in NC75sx. For Co/Ni ratios of 1 and lower, no additional phases were found in d_3 . Furthermore, the development of a γ-depleted zone can be observed, corresponding to the majority of cases closely linked to the formation of strong internal oxidation of Al [18,19]. Such zones comprise more pronounced in alloys with higher Ni contents. No continuous alumina layer was found for the investigated range of alloy compositions after 100 h exposure. Part of the available Al content already reacts to AlN which is evidently present in scales on samples with a high Co content.

In a recent study on the elementary processes during the oxidation of a ternary γ' -strengthened Co-base superalloy, individual growth kinetics for the three layers were observed [20]. To gain more information on the kinetics of multilayered scale growth in the elucidated Co/Ni-base model alloys, the thicknesses of d_1 , d_2 and d_3 were measured and plotted over exposure times. Oxide scales on specimens after 5, 12, 24, 72 and 100 h oxidation were investigated. Layer thicknesses observed on alloys with intermediate compositions, NC75sx and NC25sx, were only investigated after the maximum duration of exposure. Mean values (\bar{d}_x) of layer thicknesses are plotted over \sqrt{t} . In the following, the slope of the linear fit is referred to as k_p^{Sqr} . The fitted growth rates were used to approximate continuous data for the increase of layer thicknesses (X) with exposure time by the classical Wagner dependency (compare lines in Fig. 5).

$$X = k_p^{\text{Sqr}} \cdot \sqrt{t} \quad (1)$$

In Fig. 5, the calculated continuous increase of individual layer thickness is added as dotted line to the experimentally determined data.

The displayed average values in Fig. 5 are calculated from five separated measurements on representative locations of the cross-sections. Error bars indicate the standard deviation of the measured values. Due to the evidently low reproducibility during thermogravimetry, three experiments over the maximum duration of exposure were conducted for the pure Co-base alloy. The oxide scale of one sample spalled completely while cooling. Therefore, only the thicknesses of two samples could be measured. Both investigated oxide scales after 100 h experiments were considered for the calculation of expected scale thicknesses. Over the entire duration of isothermal exposure steady-state kinetics were not reached in the case of the pure Co-base alloys. Scattering in the determined values evidently increases with higher Co contents in the specimens. For NC50sx and NC00sx growth rates approach a steady-state between 12 and 24 h exposure. Divergent behaviour of NC50sx and the pure Ni-base alloy NC00sx become more evident after longer exposure times. The results coincide with the first conclusions drawn by means of weight gain data (Fig. 1). The dimensions of individual layers can only be compared after 100 h exposure for the complete set of considered alloys. Differences between NC00sx and NC25sx are only recognizable for the outward expansion of d_1 . Equally thick inner oxide layers grew for specimens with nominal Ni contents of more than 37.5 at.%. Interestingly, the dimensions of d_2 and d_3 found on NC75sx after 100 h oxidation almost exactly matches values determined for NC50sx. Reasons for this are most probably varying elemental transport properties depending of oxide or nature of oxide films.

The development of unwanted phases and regions significantly depleted in alloying elements in close proximity to the IOF are illustrated by BSE micrographs at different exposure times in Fig. 6.

The low stability of the γ' phase in samples with a Co/Ni ratio of 1 and higher is confirmed by the appearance of Co_3W after only 5 h of oxidation. With ongoing exposure the amount of these phases steadily increases. The large number of discrete Al-rich precipitates observed in

NC100sx is an indication for high O activity at the IOF. Following rapid progress of internal oxidation, Al is consumed in large quantities. The formation of discontinuous Al_2O_3 sections, that provide no barrier to the transport of elements can be concluded for the entire duration of exposure. Consequently, the development of a γ' -depleted region is suppressed due to the unhindered access of oxygen to the IOF. Both Ni-containing alloys, NC50sx and NC00sx, are not prone to the growth of unwanted phases. The formation of a clearly visible zone with no precipitation phase in the pure Ni-base alloy, can be mainly explained by the neglectable amount of N below the Cr-enriched barrier layer. The inward expansion of an Al-depleted region is enabled by the availability of Al, as it was not consumed by the reaction to AlN .

Since scale growth can only be sustained by transport of reactants through the growing oxide layers, kinetics during steady-state growth are approximated by the expansion of individual layers in the oxide scale. Results for k_p^{Sqr} are summarized in Table 3. At this stage it has to be alluded once again, that these values, especially for the pure Co-base alloy, are subject to rather large scatter. Repeated breakaway oxidation with subsequent healing was evidently observed during continuous monitoring of mass gain in NC100sx but might also have occurred in NC50sx.

Similar measurements were carried out by Hindam et al. to determine oxidation rates occurring during the internal and external growth of scales on the example of NiAl binary alloys [21]. Following his conclusions, the estimated growth rates (k_p^{Sqr}) for d_2 and d_3 in Table 3 are direct measures for the susceptibility to internal oxidation depending on the Co/Ni ratio, due to the occurrence of Cr-rich barrier layers in all specimens. The kinetics of d_1 are a result of the transport processes through the outer oxide layer and can therefore be directly correlated to the diffusivity of Ni/Co in the outer oxide layers.

The estimated rates of individual layer growth on NC100sx significantly exceed the k_p^{Sqr} values that were determined for specimens containing Ni. As demonstrated by the mass gain data during isothermal exposure and the subsequent examination of the oxide scale cross-section (compare Fig. 1 and 2), the pure Co-base alloy exhibits low resistance to scale formation for experiments characterised by a duration of 100 h. On the contrary, oxidation rates for the pure Ni-base alloy are comparably slow after the first 12 h of exposure. Low O permeability of the Cr-containing barrier layer is indicated by the small rate of d_2 expansion. Only minor amounts of O are observed below the diffusion-limiting barrier layer, in the pure Ni-base alloy. This is consequently expressed by the smallest k_p^{Sqr} value for the expansion of d_3 . Even though the growth rate of d_3 observed for NC50sx is higher than the growth rate of the pure Ni-base alloy, k_p^{Sqr} remains significantly below that determined for NC100sx. Diffusion velocities of Co/Ni through d_1 , sustaining the expansion of the outer oxide layer increases with higher Co contents.

As can be seen by the EPMA mappings (Fig. 3), Cr is the most essential element to the sustainment of the barrier properties of the investigated Co/Ni-base model alloys and not consumed by the formation

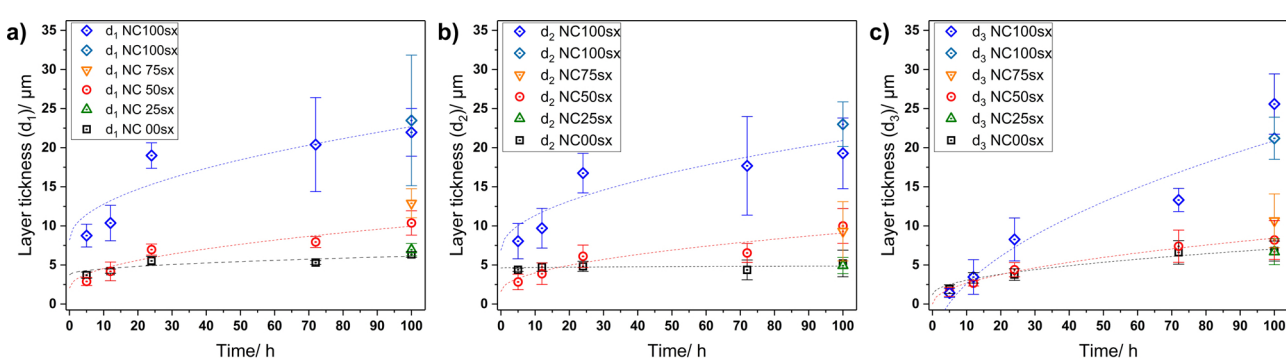


Fig. 5. Increase of individual layer thickness on Co/Ni-base model alloys at 900 °C in synthetic air as a function of exposure time. The individual layers (a) d_1 , (b) d_2 and (c) d_3 are plotted separately.

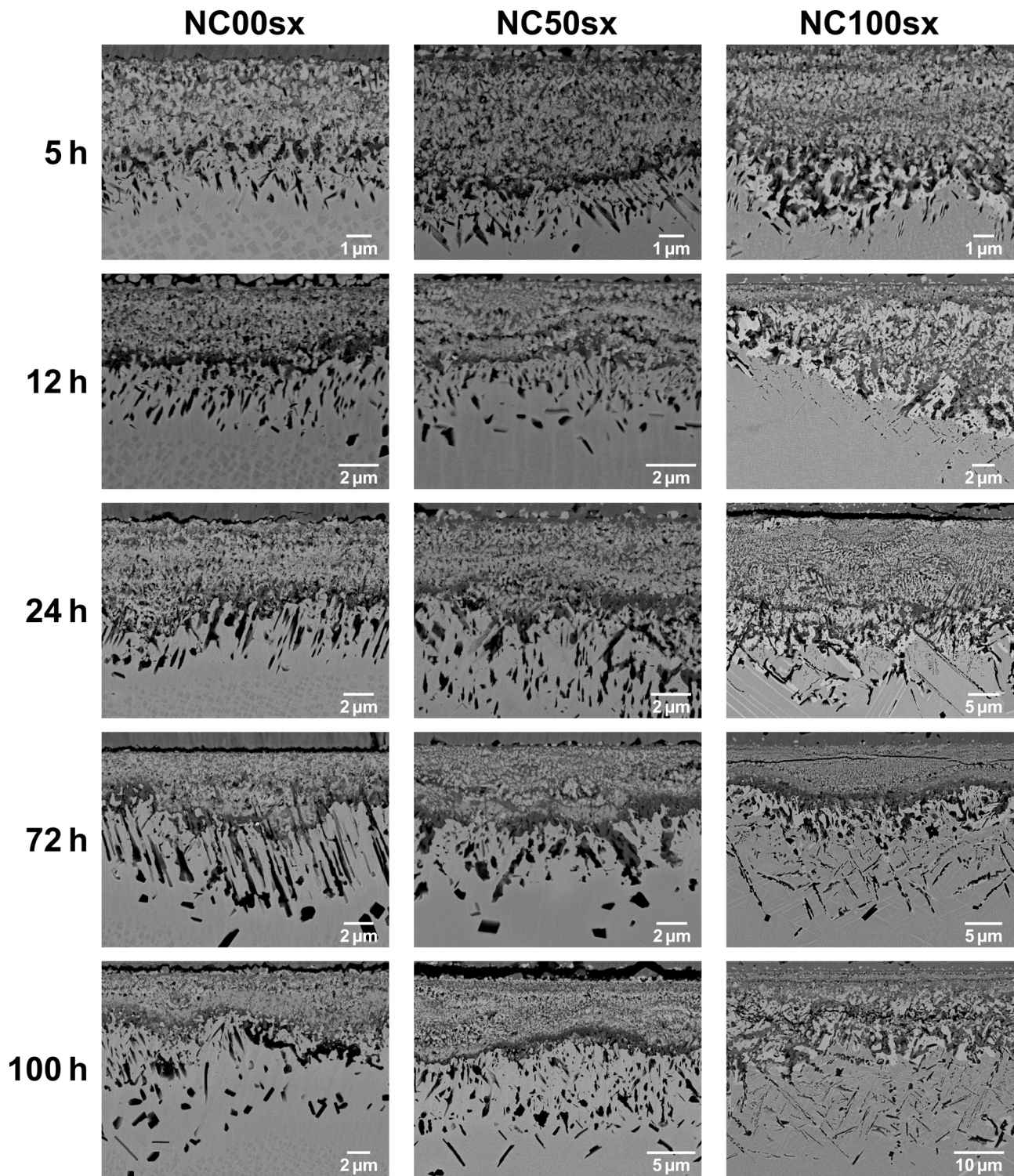


Fig. 6. Appearance of internal oxidation zone ($d_2 + d_3$) after different exposure times.

of unwanted phases. At this stage, a qualitative comparison of Cr concentration below the IOF is the only measurement that provides meaningful insight into transport processes of alloying elements depending on the Co/Ni ratio. Ideally, the continuous barrier layer corresponds to the Cr-containing oxide phases that expand the furthest into the alloy. The concentrations of Cr (in at.%) are extracted from EPMA line scans starting from the d_2/d_3 interface, moving towards the unoxidized alloy. The Cr profiles for NC100sx, NC50sx and NC00sx are plotted over the distance to the d_2/d_3 interface in Fig. 7.

A considerable decrease in the Cr content across d_3 is evident for all three samples. The formation of a Cr-rich barrier layer is accompanied by a strong decline of the d_2 growth rates. This first transition towards significantly slower kinetics is expected to occur between 12 and 24 h (compare Fig. 5) for the three considered compositions. That means, the Cr-rich layer on the d_2/d_3 interface (Fig. 3) evolved over a comparable time interval of the conducted oxidation experiment. The plotted Cr concentrations indicate a less pronounced depletion for both pure model alloys. The level of Cr in the depleted zone of NC00sx is between

Table 3

Comparison of fitted growth rates ($\mu\text{m}/\sqrt{\text{min}}$) for individual layer growth on Co-Ni model alloys at 900 °C from curve fitting between 12 and 100 h (compare Fig. 5).

Sample	$k_p^{\text{sqg}} (\mu\text{m}/\sqrt{\text{min}})$		
	d_1	d_2	d_3
NC100sx	0.197	0.181	0.345
NC50sx	0.102	0.097	0.109
NC00sx	0.031	0.003	0.076

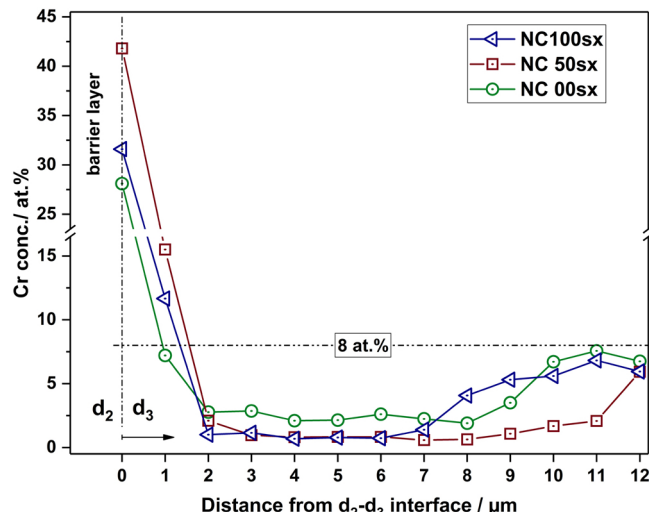


Fig. 7. Cr concentration over distance from d_2/d_3 interface. EPMA line scans were conducted from the outer oxide layer towards the unaffected alloy. Along the scan, the last measurement point that can conclusively be assigned to the Cr-containing barrier layer was designated as Cr concentration at $x = 0$. The nominal Cr concentration (8 at.%) in all alloys is indicated by a horizontal line.

2 and 3 at.%, whereas the Co-containing alloys exhibit Cr contents below 1 at.% in these regions. From the presented data, the highest diffusivity of Cr can be concluded in the intermediate Co/Ni-base alloy NC50sx at 900 °C.

3.4. Efficacy of the halogen effect

So far, oxidation resistance of all investigated alloys can be assessed as insufficient for potential usage at 900 °C and above. To overcome these limitations, near-surface regions of all samples were doped with F to initiate external growth of protective alumina oxide scales. The efficacy of such treatment was evaluated by isothermal exposure in synthetic air for 100 h at 900 °C. The oxide scale structures and the distribution of elements in the oxidation-affected regions are displayed in Fig. 8. For untreated samples, the cross-sections observed on NC25sx and NC75sx demonstrated only minor differences compared to the pure Ni- or Co-containing samples and were therefore not included in the summary of elemental distributions (compare Fig. 3).

The oxide scale observed on the pure Co-base alloy (Fig. 8a) exhibited a comparable appearance to the one found on untreated NC100sx. Nevertheless, a Cr-containing barrier layer followed by an Al_2O_3 layer was observed in the investigated region of the sample. For the NC75sx sample (Fig. 8b), the pretreatment remained without effect on the oxidation behaviour. A substantially thick outer oxide layer that consists of Co, Ni and O was observed above the original alloy surface. Towards the d_2/d_3 interface, a discontinuous Cr-rich barrier layer forms. Below this interface, Al-rich precipitates of AlN are found.

EPMA mappings reveal a beneficial effect of halogen treatments for

the alloy with equal Co and Ni contents. Below the Cr-containing barrier layer, that was already apparent in the untreated sample after 100 h exposure, additional formation of a continuous Al_2O_3 layer was observed. The substantially lower overall thickness of the oxide scale accounts for a faster transition between internal to external scale growth facilitated by F doping prior to thermal exposure in synthetic air. Interestingly, both samples, NC50sx and NC100sx exhibited widely comparable behaviour during isothermal exposure at 900 °C after F treatment. Higher oxidation resistance could be achieved for these compositions, even though it was not possible to promote the development of an external protective layer already during the very early stages of scale formation.

Electron micrographs of the oxidised cross-sections demonstrate a beneficial effect of the surface pretreatment in terms of oxidation resistance for the Ni-rich alloys NC25sx and NC00sx (Fig. 8d and e). In both cases the grown oxide scale is significantly thinner than on the untreated surface. After treatment with halogens, the section of NC25sx that is displayed in the elemental mappings consists almost exclusively of protective oxides. Compared to the oxide layer that were observed on the pure Ni-base alloy a larger fraction of the surface is covered by initially grown Al_2O_3 (Fig. 8d). On the remaining fractions of the surface an external Cr_2O_3 scale is apparent. Although the displayed micrographs show $(\text{Ni}, \text{Co})\text{O}$ in negligible small portions, the investigated sample exhibits a certain extend of this non-protective oxide phase on the outer scale interface. The distribution of W in the Co-containing NC25sx alloy is similar to the one observed for the pure Ni-base alloy.

The oxide scales on NC00sx still reveal a multilayered structure with a thin NiO layer covering most of the surface, but an exclusive external Al_2O_3 growth could not be promoted by the pretreatment. On the right-hand side of the displayed elemental mapping, the Al_2O_3 barrier layer was initially formed on the exposed surface, whereas the remaining cross-section is covered by an outer NiO -layer. The internal oxidation zone is a Cr-containing barrier layer, that is followed by Al_2O_3 . Below the alumina layer, AlN precipitates are visible.

4. Discussion

4.1. Scale growth on untreated Co/Ni-base alloys

Oxidation behaviour of single-crystalline Co/Ni-base alloys obeyed the same general trend reported for their polycrystalline counterparts [9]. Furthermore, many publications already pointed out the low phase-stability of ternary and quaternary Co-base alloys without the addition of Ni during oxidation at temperatures above 800 °C [22–25]. Depletion of Al coincides with the growth of an unwanted intermetallic Co_3W phase. The narrow compositional window in which the desired γ/γ' microstructure can be sustained is a major drawback that limits the usability of Co-base alloys. Nevertheless, the addition of Ni is known to widen the γ/γ' two-phase region [7]. Therefore, a higher tolerance of the unoxidized substrate towards Al depletion was obtained with increasing Ni content in the investigated alloys. Furthermore, higher Ni content significantly improves the resistance against oxidation and consequently lowers the detected weight change during thermogravimetry at 900 °C.

Throughout this study, the development of Cr-containing barrier layer was demonstrated to be of crucial importance for the overall oxidation behaviour. For binary Co-Cr alloys, that include a Cr content below 20 at.%, the formation of CoCr_2O_4 spinel phases was reported in literature [26–28]. Only for higher Cr contents (20–30 at.%), the formation of a thin Cr_2O_3 layer below the spinel layer was observed [27]. Nevertheless, a considerable blocking effect of continuous spinel layers was observed in binary Co-Cr alloys [29]. Due to the intermediate Cr content of 8 at.% in the investigated alloys, the Cr-rich layer can be expected to consist primarily of CoCr_2O_4 for NC100sx. Reviewing the available literature, the observed Cr-containing barrier layer in NC00sx after 100 h exposure at 900 °C is mainly composed of a Ni-Cr spinel

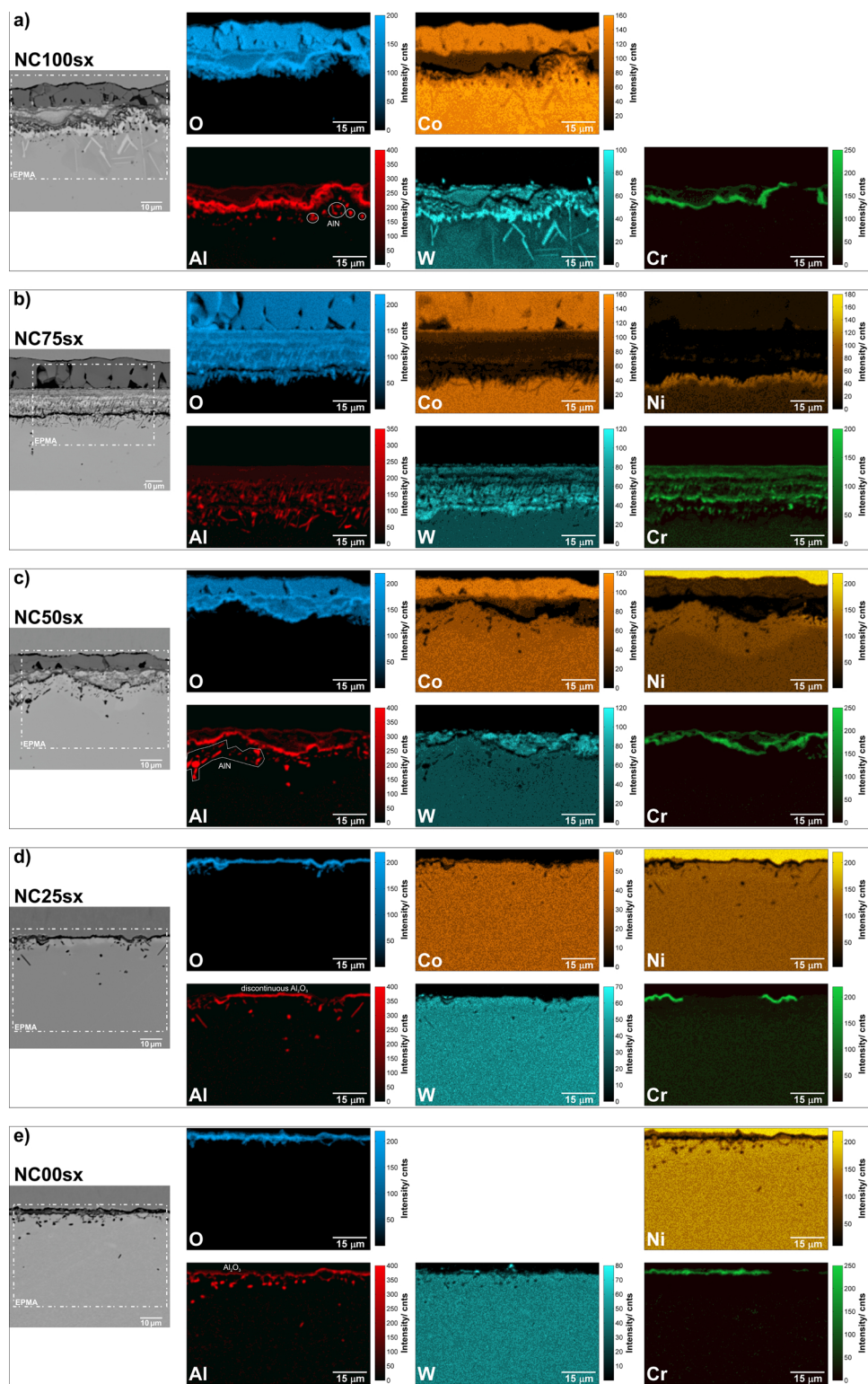


Fig. 8. SEM micrographs of oxide scales grown on F-implanted surfaces. Elemental distribution in the marked (–) region were determined by EPMA.

phase. Several studies pointed out the solid state reaction between NiO and Cr_2O_3 , that can lead to the formation of NiCr_2O_4 in binary Ni-Cr alloys [30,31]. Similar to the Co-Cr spinel, diffusion was observed to be effectively reduced by the formation of a continuous NiCr_2O_4 layer [29,31,32].

Formation of a Cr-containing diffusion barrier was also observed for the intermediate Co/Ni-base model alloy NC50sx. The identification of all developed oxide phases during the isothermal exposure in the inner

oxide layer on this relatively complex model alloys, is beyond the scope of this study. However, the products of internal oxidation during the high-temperature exposure of Co-Cr-Al and Ni-Cr-Al systems were subject to several previous studies (e.g. [29,33]). After carefully reviewing the available literature, formation of $(\text{Co}/\text{Ni})\text{Cr}_2\text{O}_4$ spinel layers at the d_2/d_3 interface seems highly probable in all (model) alloys that contain intermediate Cr and Al (< 10 at.%) contents [28,34–38]. Depletion of Co accompanied by an apparent increase in Ni, is visible in

the uppermost region of d_3 in NC50sx after 100 h exposure. Since the alloy initially contained equal Co and Ni contents, these findings indicate that the outward flux of Co, compared to Ni, is considerably faster.

Scatter of data increased for higher Co contents in the alloys and is particularly pronounced for the pure Co-base alloy. As already mentioned above, three NC100sx samples were oxidized for 100 h in the TGA. One sample showed significant higher increase in weight without the formation of any Cr-containing barrier layer. The other two investigated samples exhibited considerable sections of barrier layers. Poor reproducibility was already demonstrated for Co-Cr-Al model alloys at elevated temperatures [39,40]. Differences in the recorded mass gain curves can be directly correlated with the formation of diffusion-limiting, Cr-containing layers. Furthermore, local failure of protective scale sections are recognisable by sudden increases in the weight gain curves (compare Fig. 1). During such events, the initially formed barrier layer could not sustain its properties over the entire duration of exposure. For the set of investigated alloys, the oxidation rate is also observed to decline again, which indicates (repeated) healing of the cracked regions. The failure of barrier layer might have specific consequences for the content of Cr below this interface. As described in classical model on the cracking of expanding oxide scales [41,42], metal activity under the more oxygen-permeable scale region can no longer be sustained. Consequently, Cr diffuses more extensively towards the failed interface. An experimental proof can be found in the EPMA concentration profiles in Fig. 7. For NC100sx and NC50sx, considerably higher amounts of Cr are consumed during the repeated healing of cracks inside the barrier layer and therefore a region of negligible Cr concentration spreads approximately 5–7 μm into the internal precipitation zone. From a different perspective, one can assume that in average more O is available at the d_2/d_3 interface during the entire 100 h of exposure at 900 °C. Even though, the intermediate Co/Ni alloy NC75sx did not show significant discrepancies during the two conducted thermogravimetric experiments, onset of considerable barrier layer formation cannot be absolutely excluded since local variations of Cr might be enough for the development of continuous Co-Cr-spinel sections in the internal oxidation zone.

Long-term stability and oxidation resistance of Co-Cr alloys were already subject to several studies in the literature. Stott et al. compared the oxidation behaviour of M-Cr-Al (M = Ni, Fe, Co) model alloys between 1000 and 1200 °C. In this early study, Ni-base alloys containing intermediate Cr (10–15 at.%) and Al (0.9–1.3 at.%) contents already exhibited superior adherence and therefore less susceptibility to scale failure cracking of the initially formed protective layers [40]. However, it has to be noted that significant discrepancies were observed between the calculated and experimentally determined values for the minimum Cr concentration that is required to form a protective Cr_3O_3 layer in binary Ni-Cr alloys [33]. In order to explain these differences, transport of alloying elements to the advancing reaction front has to be considered. The initially formed, thermodynamically most stable phases in the investigated model alloys are Al_2O_3 and Cr_2O_3 . Following the depletion of for example Cr in the sub-surface zone, the activity of Cr on the IOF can fall below the required value to sustain growth of a protective Cr_2O_3 layer. Consequently, the initially developed chromia reacts to the NiCr_2O_4 spinel phase. Rapid transport of O leads to a high O activity above the d_2/d_3 interface. Large gradients of elemental activity across chromia scales are known to decrease the long-term resistance against internal oxidation in Co/Ni-base model alloys [43]. Due to the described kinetic considerations, the formation of Cr-containing spinels can be expected to occur regardless of the base element. To suppress the development of spinel phases and guarantee higher oxidation resistance, a sufficiently high concentration of Al/Cr in the alloy is needed to sustain the required activity at the d_2/d_3 interface.

Higher stability of the desired γ/γ' structure in sub-scale regions with increasing Ni content was apparent throughout the present study. A previous study on the thermophysical properties of polycrystalline

Co/Ni-base model alloys already introduced the unique features of the two-phase microstructure, depending on the Co/Ni ratio in detail [9]. Nevertheless, the study did not comment on phase changes that were induced by transport of alloying elements to the IOF as a consequence of thermal exposure. Despite the broadening of the two-phase field due to the addition of 19.8 at.% Ni in NC75sx, unwanted formation of thin Co_3W needles (compare Fig. 2) adjacent to Al_2O_3 or AlN precipitates was observed after 100 h exposure. In alloys with higher Ni levels, no undesired Co_3W needles formed over the entire duration of exposure. The occurrence of nitrides in d_3 during oxidation of untreated Co/Ni-base alloys in air is also evidently dependent on the Ni content. For example a huge amount of long needle-like AlN precipitates was apparent in NC100sx, regardless of whether a continuous Cr-containing barrier layer had established at the d_2/d_3 interface or not (compare Fig. 3a and b). Over the last decades, several studies pointed out the insufficient resistance against oxide scale formation of Co- or Ni-base alloys that were solely protected by Cr_2O_3 barrier layers. Penetration of N could be demonstrated to be a core issue, especially for environments with low oxygen contents [44–46]. Additionally, Han et al. even observed considerable formation of AlN and Cr_2N below a continuous $\text{Cr}_2\text{O}_3\text{-Al}_2\text{O}_3$ scale during cyclic oxidation in lab air [47]. In their study, the authors associated the severe nitridation with repeated cracking of the initially protective oxide scale during the thermal cycling. The growth of AlN precipitates during the oxidation of Co/Ni-base alloys was explainable by its higher free energy of formation compared to Cr_2N [47]. In the investigated Co/Ni-base alloy system, cracking of diffusion-limiting scale sections could be demonstrated to be a serious problem for Co-containing samples (compare Fig. 3a-c). The N permeability of Cr-rich barrier layer is evidently dependent on the Co/Ni ratio in the alloy and decreases with increasing Ni content. As mentioned above, chromia-forming Co-Cr alloys were repeatedly reported to suffer from scale failure even under isothermal conditions [39].

4.2. Transport of reactants depending on alloy composition

To fully elucidate the oxidation behaviour of Co/Ni-base model alloys, mass transport through the scale and adjacent alloy regions has to be considered. The outer oxide layers that were observed are either CoO or NiO or a solid solution of $(\text{Co},\text{Ni})\text{O}$. Transport of Ni and/or Co was subject to a recent study using oxygen tracer exchange experiments. Metal cations could be demonstrated to diffuse mainly via the oxide lattice [48]. Clear evidences for decreasing oxidation rates of Co/Ni binary alloys with increasing Ni contents can be found in the literature [49,50]. Both studies assigned faster material transport through the outer oxide scale to prevailing defect densities in these layers on the Co-rich side. For the set of investigated Co/Ni-base alloys, comparable mechanisms for the outward growth of d_1 can be assumed.

The development of an internal oxidation zone on the other hand is driven by transport of oxygen through d_1 towards the d_2/d_3 interface respectively. At this stage the exact transport mechanisms remain unclear. The conditions which have to be fulfilled for the formation of a lateral growing, protective layer, were already qualitatively postulated by Wagner [51]. A sufficiently high flux of the thermodynamically more stable scale former, in this case Cr or Al, needs to be sustained from adjacent regions of the alloy. In other words, at a given flux of oxygen, diffusion velocities of Al and Cr inside the alloy are of essential importance. As stated above, the estimated k_p^{SQR} values for the expansion of d_2 and d_3 are direct measures for the relative permeability of O (and N) through the multilayered scale. Due to the high free energy of formation, Al_2O_3 is the first oxide that is formed. The observation of mostly discrete precipitates instead of layer sections (Fig. 3) that spread parallel to the original alloy surface accounts for the insufficient flux of Al. Since a significant amount of Al is consumed by the growth of these Al_2O_3 precipitates, that consequently lower the oxygen partial pressure in this region, Cr can diffuse to the d_2/d_3 interface to finally form a continuous layer. The width of the developed Cr-depleted zone

underneath is depending on the mobility of Cr in the alloy. From Fig. 7, the highest Cr diffusivity can be concluded for the intermediate Ni/Co-base alloy NC50sx. Several authors determined the diffusion coefficients for Cr and W in pure binary Co and Ni alloys [52,53]. From this studies, Cr diffusion in the pure Ni-base model alloy can be estimated to be higher than in the pure Co-base counterpart at 900 °C. This trend was also observed in the EPMA line scans across the Cr-depleted regions (compare Fig. 7). The more pronounced depletion of Cr in the intermediate Co/Ni-base alloy suggests a higher diffusion coefficient, that would be beneficial for the formation of a protective Cr_2O_3 layer and consequently result in an increased oxidation resistance. The overall higher Cr content in the depleted zone of NC00sx is an indication for more effective barrier properties of the diffusion-limiting layer. Therefore, this layer on the alloy can be expected to sustain longer.

4.3. Altered oxide growth after F implantation

After surface doping with fluorine the individual thickness of oxide layers and the appearance of protective scale sections significantly changes. Especially on the Ni-rich side, external (Al_2O_3) scale formation can be triggered (compare Fig. 3 and 8). Interestingly, not only the desired alumina layer that forms for example on titaniumaluminides (TiAl) after optimised fluoridation [12–14], but also an external growth of chromia scale sections can be locally observed (most pronounced for NC25sx). This finding clearly indicates that the underlying mechanism found in this study demonstrated higher complexity compared to F-treated TiAl systems. On the Co-rich side, the halogen effect is less effective. Even though, the Al_2O_3 formation is clearly affected, no external scale establishes. The faster growth of CoO compared to NiO [49,50] only allows a shorter period for the enrichment of Al on the surface before considerable consumption of the base metal proceeds. Nevertheless, the presented results found for the pure Co-base alloy are still highly intriguing. It could be demonstrated that the halogen effect can be used to modify the scale formation on this model alloy system with initially low oxidation resistance. However, more detailed studies are needed to optimise the applied parameters for the ion implantation. Already this first elucidation of the halogen effect on the investigated Co/Ni-base model alloys demonstrated further, new aspects such as the impact of the treatment on the mobility of Cr, that provides a fascinating starting point for future studies.

5. Conclusions

In the present study the role of the Co to Ni ratio for the scale growth and the efficacy of the halogen effect was investigated in high detail.

The oxidation behaviour of Cr-containing Co/Ni-base model alloys was obtained to be a complex interplay between exposure temperature and the ratio of considered base elements. At 900 °C, weight gain increases with higher Co contents in the investigated alloys. All exposed samples demonstrated the development of three-layered oxide scales. Generally, a certain degree of resistance was achieved by Cr-rich spinels that formed barrier layers on the IOF after a period of initially rapid reaction kinetics.

Extensive formation of nitrides occurred on model alloys with a nominal Co content of 37.5 at.% and higher. The observed differences in oxidation behaviour could be directly attributed to changes of Al and Cr mobilities caused by the individual levels of base elements. Significant depletion of Al and Cr in sub-scale region was accompanied by the decay of the γ/γ' phase and the development of unwanted Co_3W for alloys with higher Co contents. Furthermore, the sustainability of the barrier layers was limited for alloys with a Co/Ni ratio of 1 and higher.

The halogen effect was demonstrated to strongly affect transport properties of Al and Cr in all investigated alloys. For high Ni contents, the external growth of protective $\text{Al}_2\text{O}_3/\text{Cr}_2\text{O}_3$ scales could be

facilitated by ion-implantation with fluorides prior to thermal exposure. In the pure Co-base model alloy, Al was enriched in the sub-surface region, but the formation of an external alumina layer was suppressed due to the overall faster growth kinetics of CoO at the given temperature. Consequently, it is worth to further investigate the effect of halogen treatment for this relatively new type of high-temperature material in more detail.

Acknowledgments

Scientific and financial support by the Deutsche Forschungsgemeinschaft (DFG) through the Collaborative Research Centre SFB-TR 103 (Project A5 and B3) is highly acknowledged. The authors would like to express their thanks to Gerald Schmidt for sophisticated EPMA measurements. CHZ acknowledges financial support through the Alexander von Humboldt Foundation.

References

- [1] B. Pint, J. DiStefano, I. Wright, Oxidation resistance: one barrier to moving beyond Ni-base superalloys, Mater. Sci. Eng. A 415 (2006) 255–263.
- [2] J. Sato, T. Omori, K. Oikawa, I. Ohnuma, R. Kainuma, K. Ishida, Cobalt-base high-temperature alloys, Science 312 (2006) 90–91.
- [3] A. Suzuki, T. Pollock, High-temperature strength and deformation of γ/γ' two-phase Co-Al-W base alloys, Acta Mater. 56 (2008) 1288–1297.
- [4] A. Bauer, S. Neumeier, F. Pyczak, M. Göken, Microstructure and creep strength of different γ/γ' – strengthened Co-base superalloy variants, Scr. Mater. 63 (2010) 1197–1200.
- [5] A. Bauer, S. Neumeier, F. Pyczak, R. Singer, M. Göken, Creep properties of different γ' – strengthened Co-base superalloys, Mater. Sci. Eng. A 550 (2012) 333–341.
- [6] E.A. Lass, M.E. Williams, C.E. Campbell, K.-W. Moon, U.R. Kattner, γ' phase stability and phase equilibrium in ternary Co-Al-W at 900 °C, J. Phase Equilif. Diffusion 35 (2014) 711–723.
- [7] K. Shinagawa, T. Omori, J. Sato, K. Oikawa, I. Ohnuma, R. Kainuma, K. Ishida, Phase equilibria and microstructure on γ' phase in Co-Ni-Al-W system, Mater. Trans. 49 (2008) 1474–1479.
- [8] L. Klein, M. Killian, S. Virtanen, The effect of nickel and silicon addition on some oxidation properties of novel Co-based high temperature alloys, Corros. Sci. 69 (2013) 43–49.
- [9] C. Zenk, S. Neumeier, N. Engl, S. Fries, O. Dolotko, M. Weiser, S. Virtanen, M. Göken, Intermediate Co/Ni-base model superalloys – thermophysical properties, creep and oxidation, Scr. Mater. 112 (2016) 83–86.
- [10] C. Zenk, S. Neumeier, M. Kolb, N. Volz, S. Fries, O. Dolotko, I. Povstugar, D. Raabe, M. Göken, The role of the base element in γ' strengthened cobalt/nickel-base superalloys, Proceedings of the International Symposium on Superalloys (2016).
- [11] S. Kobayashi, Y. Tsukamoto, T. Takasugi, H. Chinen, T. Omori, K. Ishida, S. Zaefferer, Determination of phase equilibria in the Co-rich Co-Al-W ternary system with a diffusion-couple technique, Intermetallics 17 (2009) 1085–1089.
- [12] H.-E. Zschau, V. Gauthier, G. Schumacher, F. Dettenwanger, M. Schütze, H. Baumann, K. Bethge, M. Graham, Investigation of the fluorine microalloying effect in the oxidation of TiAl at 900 °C in air, Oxid. Met. 59 (2003) 183–200.
- [13] H.-E. Zschau, M. Schütze, H. Baumann, K. Bethge, The time behaviour of surface applied fluorine inducing the formation of an alumina scale on gamma-TiAl during oxidation at 900 °C in air, Intermetallics 14 (2006) 1136–1142.
- [14] H.-E. Zschau, M. Schütze, H. Baumann, K. Bethge, Surface modification of titanium aluminides with fluorine to improve their application for high temperature service conditions, Nucl. Instrum. Methods Phys. Res., Sect. B: Beam Interact. Mater. Atoms 257 (2007) 383–387.
- [15] H.-E. Zschau, P. Masset, M. Schütze, The halogen effect for Ni-base superalloys – a thermodynamic study, Mater. Sci. Forum 638–642 (2010) 2375–2380.
- [16] H.-E. Zschau, P. Masset, M. Schütze, Oxidation protection of Ni-base superalloys by halogen treatment, Mater. Corros. 62 (2011) 687–694.
- [17] H.-E. Zschau, W. Zhao, S. Neve, B. Gleeson, M. Schütze, Promotion of the Al_2O_3 -scale formation on Ni-Cr-Al alloys via the fluorine effect, Oxid. Met. 83 (2015) 335–349.
- [18] M. Levy, P. Farrell, F. Pettit, Oxidation of some advanced single-crystal nickel-base superalloys in air at 2000 F(1093 C), Corrosion 42 (1986) 708–717.
- [19] B. Pieraggi, F. Dabosi, High-temperature oxidation of a single crystal Ni-base superalloy, Werkstoffe Korrosion 38 (1987) 584–590.
- [20] M. Weiser, Y. Eggeler, E. Specker, S. Virtanen, Early stages of scale formation during oxidation of γ/γ' strengthened single crystal ternary Co-base superalloy at 900 °C, Corros. Sci. 135 (2018) 78–86.
- [21] H. Hindam, W. Smeltzer, H. Hindam, Growth and microstructure of $\alpha\text{-Al}_2\text{O}_3$ on $\beta\text{-NiAl}$ alloys: internal precipitation and transition to external scale, J. Electrochem. Soc. 127 (1980) 1622–1630.
- [22] T. Pollock, J. Dibbern, M. Tsunekane, J. Zhu, A. Suzuki, New Co-based $\gamma - \gamma'$ high-temperature alloys, JOM 62 (2010) 58–63.
- [23] L. Klein, Y. Shen, M. Killian, S. Virtanen, Effect of B and Cr on the high temperature oxidation behaviour of novel γ/γ' -strengthened Co-base superalloys, Corros. Sci. 53 (2011) 2713–2720.

- [24] L. Klein, A. Bauer, S. Neumeier, M. Göken, S. Virtanen, High temperature oxidation of γ/γ' – strengthened Co-base superalloys, *Corros. Sci.* 53 (2011) 2027–2034.
- [25] H.-Y. Yan, V. Vorontsov, D. Dye, Effect of alloying on the oxidation behaviour of Co-Al-W superalloys, *Corros. Sci.* 83 (2014) 382–395.
- [26] P.K. Kofstad, A.Z. Hed, Oxidation of Co-25 w/o Cr at high temperatures, *J. Electrochem. Soc.* 116 (1969) 1542–1550.
- [27] I. Wright, G. Wood, The isothermal oxidation of Co-Cr alloys in 760 Torr oxygen at 1000 °C, *Oxid. Met.* 11 (1977) 163–191.
- [28] P. Hou, The effect of surface-applied reactive element oxide on the oxidation of binary alloys containing Cr, *J. Electrochem. Soc.* 134 (1987) 1836–1849.
- [29] G. Wallwork, A. Hed, Some limiting factors in the use of alloys at high temperatures, *Oxid. Met.* 3 (1971) 171–184.
- [30] G. Wood, T. Hodgkiess, Mechanism of oxidation of dilute nickel-chromium alloys, *Nature* 211 (1966) 1358–1361.
- [31] C. Giggins, F. Pettit, Oxidation of Ni-Cr-Al alloys between 1000 °C and 1200 °C, *J. Electrochem. Soc.* 118 (1971) 1782–1790.
- [32] D.L. Douglass, J.S. Armijo, The effect of silicon and manganese on the oxidation mechanism of Ni-20 Cr, *Oxid. Metals* 2 (1970) 207–231.
- [33] A. Dalvi, D. Coates, A review of the diffusion path concept and its application to the high-temperature oxidation of binary alloys, *Oxid. Met.* 5 (1972) 113–135.
- [34] J.E. Croll, G.R. Wallwork, The design of iron-chromium-nickel alloys for use at high temperatures, *Oxid. Met.* 1 (1969) 55–71.
- [35] P. Kofstad, A. Hed, High-temperature oxidation of Co-10 w/o Cr alloys, *J. Electrochem. Soc.* 116 (1969) 224–234.
- [36] G. Giggins, F. Pettit, Oxidation of Ni-Cr alloys between 800 °C and 1200 °C, *Trans. Metallur. Soc. AIME* 245 (1969) 2495–2507.
- [37] G. Irving, J. Stringer, D. Whittle, The oxidation of Co-20% Cr base alloys containing Nb or Ta, *Corros. Sci.* 15 (1975) 337–344.
- [38] P. Hou, J. Stringer, The effect of surface-applied reactive metal oxides on the high temperature oxidation of alloys, *Mater. Sci. Eng.* 87 (1987) 295–302.
- [39] G. Wood, F. Stott, The influence of aluminum additions on the oxidation of Co-Cr alloys at 1000 and 1200 °C, *Oxid. Met.* 3 (1971) 365–398.
- [40] F. Stott, G. Wood, M. Hobby, A comparison of the oxidation behavior of Fe-Cr-Al, Ni-Cr-Al, and Co-Cr-Al alloys, *Oxid. Met.* 3 (1971) 103–113.
- [41] S. Mrowec, On the mechanism of high temperature oxidation of metals and alloys, *Corros. Sci.* 7 (1967) 563–578.
- [42] G.B. Gibbs, A model for mild steel oxidation in CO₂, *Oxid. Met.* 7 (1973) 173–184.
- [43] G. Wood, I. Wright, T. Hodkiess, D. Whittle, A comparison of the oxidation of Fe-Cr, Ni-Cr and Co-Cr alloys in oxygen and water vapour, *Werkstoffe Korrosion* 21 (1970) 900–910.
- [44] I.C. Chen, D.L. Douglass, The internal nitriding behavior of Co-3Cr, Co-3Al, and Co-3Ti (a/o) over the range of 700–1100 °C, *Oxid. Met.* 38 (1992) 189–205.
- [45] U. Krupp, H.-J. Christ, Internal nitridation of nickel-base alloys. Part I. Behavior of binary and ternary alloys of the Ni-Cr-Al-Ti system, *Oxid. Met.* 52 (1999) 277–298.
- [46] U. Krupp, H.-J. Christ, Internal nitridation of nickel-base alloys. Part II. Behavior of quaternary Ni-Cr-Al-Ti alloys and computer-based description, *Oxid. Met.* 52 (1999) 299–320.
- [47] S. Han, D. Young, Simultaneous internal oxidation and nitridation of Ni-Cr-Al alloys, *Oxid. Met.* 55 (2001) 223–242.
- [48] R. Chater, M. Weiser, S. Virtanen, Visualizing ion transport mechanisms through oxide scales grown on mixed nickel- and cobalt-base model alloys at 900 °C using FIB-SIMS techniques, *J. Vac. Sci. Technol. B: Nanotechnol. Microelectron.* 36 (2018).
- [49] G. Wood, I. Wright, J. Ferguson, The oxidation of Ni and Co and of Ni/Co alloys at high temperatures, *Corros. Sci.* 5 (1965) 645–661.
- [50] K. Nishida, T. Narita, N. Ohya, T. Yamauchi, Oxidation kinetics and scale structures of Co-Ni alloys in the temperature range from 1000 to 1200 °C, *Trans. Jpn. Inst. Met.* 16 (1975) 755–765.
- [51] C. Wagner, Reaktionstypen bei der Oxydation von Legierungen, *Zeitschrift für Elektrochemie, Berichte der Bunsengesellschaft für physikalische Chemie* 63 (1959) 772–782.
- [52] A. Davin, V. Leroy, D. Coutsouradis, L. Habraken, Diffusion de quelques éléments de substitution dans le fer, le nickel et le cobalt, *Mémoires scientifiques de la Revue de métallurgie* 60 (1963) 275–283.
- [53] S. Neumeier, H. Rehman, J. Neuner, C. Zenk, S. Michel, S. Schuwallow, J. Rogal, R. Drautz, M. Göken, Diffusion of solutes in fcc Cobalt investigated by diffusion couples and first principles kinetic Monte Carlo, *Acta Mater.* 106 (2016) 304–312.